Taylor & Francis
Taylor & Francis Group

Chemical Engineering Communications

ISSN: 0098-6445 (Print) 1563-5201 (Online) Journal homepage: http://www.tandfonline.com/loi/gcec20

Viscous Filament Fragmentation in a Turbulent Flow Inside a Stirred Tank

René Sanjuan-Galindo, Enrique Soto, Roberto Zenit & Gabriel Ascanio

To cite this article: René Sanjuan-Galindo, Enrique Soto, Roberto Zenit & Gabriel Ascanio (2015) Viscous Filament Fragmentation in a Turbulent Flow Inside a Stirred Tank, Chemical Engineering Communications, 202:9, 1251-1260, DOI: 10.1080/00986445.2014.923994

To link to this article: http://dx.doi.org/10.1080/00986445.2014.923994

Chemical Engineering Communications, 202:1251–1260, 2015

ISSN: 0098-6445 print/1563-5201 online
DOI: 10.1080/00986445.2014.923994

Taylor & Francis
Taylor & Francis Group

Viscous Filament Fragmentation in a Turbulent Flow Inside a Stirred Tank

RENÉ SANJUAN-GALINDO[1], ENRIQUE SOTO[2], ROBERTO ZENIT[3], and GABRIEL ASCANIO[2]

[1]*Centro de Investigación e Innovación Tecnológica, Instituto Tecnológico de Nuevo León, Apodaca, Mexico*
[2]*Centro de Ciencias Aplicadas y Desarrollo Tecnológico, Universidad Nacional Autónoma de México, Mexico City, Mexico*
[3]*Instituto de Investigaciones en Materiales, Universidad Nacional Autónoma de México, DF, Mexico*

The present work describes the dispersion process of a viscous fluid in water in a cylindrical vessel agitated at Re = 24,000. The formation of viscous filaments and other amorphous structures in turbulent conditions produced in the early stage, before oil drops saturate the continuous phase, is shown. The oil-phase evolution is followed with high-speed video recordings and compared with the flow pattern produce in the liquid bulk. The effects of four kinds of perturbations are identified: intermittences in the radial velocity, turbulent fluctuations, rotation, and the stretching. As a consequence, the viscous-phase experiences instabilities that include random deformation, elongation, hairpin filaments formation, folding, and fragmentation. In the final part of this study, a mechanism describing the drop size reduction has been proposed.

Keywords: Oil filaments; Stirred tank; Turbulent flow; Viscous structures

Introduction

The dispersion of two immiscible liquids (i.e., oil-in-water dispersion) is a common unit operation in pharmaceutics, biochemistry, food processing, and other industrial sectors. The production of dispersions are the result of the necessity to prepare meals, paints and powders; in industry, dispersions are commonly prepared in stirred tanks to obtain size reduced droplets dispersed in a continuous phase with the aim of increasing the interfacial contact between the two liquids. This system is thermodynamically unstable even though the mass transfer and the energy transfer are enhanced; that is why, many authors have tested liquid–liquid dispersions in a wide range of conditions—for instance, by modifying the interfacial tension, the concentration or the viscosity ratio between the two liquids (Coulaloglou and Tavlarides, 1976; Wang and Calabrese, 1986; Zhou and Kresta, 1998; Lovick et al., 2005). However, in most of these studies, dispersions have been monitored by following the drop size distribution, so that the mechanism did not occur before the formation of drops. Such a mechanism occurs in the beginning of the process in a short period of time, involving the stretching and fragmentation of the viscous-phase producing filaments.

Address correspondence to Gabriel Ascanio, Centro de Ciencias Aplicadas y Desarrollo Tecnológico, Universidad Nacional Autónoma de México. Apdo. Postal 70-186, 04510 México D.F., México. E-mail: gabriel.ascanio@ccadet.unam.mx

Color versions of one or more of the figures in the article can be found online at www.tandfonline.com/gcec.

Filaments are time-dependent fluid threads moving in a fluid stream, being this phenomenon known as tangential separation; such a phenomenon is present in many quotidian events such as honey threads in an air stream or silicone filaments dragged in water. Plateau (1849) and Rayleigh (1892) were the first to study the hydrodynamic instability of thin threads. The Plateau–Rayleigh instability consists of undulations produced by capillary effects. Although in industrial applications, threads are perturbed by turbulent inertial forces, in most of the scientific literature filaments exposed to shear-free flows at very low flow regimes (i.e., $Re \approx 1$) have been investigated (Tjahjdadi and Ottino, 1991; Skorobogatiy and Mahadevan, 2000; Ribe, 2004; Le Merrer et al., 2008). Yarin (1997) modeled the dynamics of non-Newtonian stretched filaments exposed to shear flow. Instabilities on confined filaments were analyzed by Hagedorn et al. (2004), while the effects of gravitational, inertial, and viscous forces were reported by Skorobogatiy and Mahadevan (2000), Ribe (2004), and Duclaux et al. (2006). The folding of the dispersed phase is the result of competition between the external flow, the gravitational forces and the viscous forces (Skorobogatiy and Mahadevan, 2000). In such a process, the filament cross section reduces heterogeneously causing longitudinal rearrangements or breakage (Oliveira and McKinley, 2005). Eggers and Villermaux (2008) discussed several types of perturbations like the transition from dripping to jetting, a co-flowing liquid stream or the effect of the velocity differences between the filament and its surroundings. Lueptow and Lueptow (2012) reported the instabilities of honey filaments as they were poured into quiescent water.

Even though the production of filaments is common in industrial processes, the occurrence of such a phenomenon inside a stirred tank has not been widely documented. To achieve the dispersion of the two immiscible liquids, both turbulent conditions and high fluctuations in the flow field are needed (Mathieu and Scott, 2000; Sajjadi et al., 2002). The flow structure depends on the type, position, and number of impellers (as well as the direction and magnitude of the rotational speed) and the presence of baffles (used to inhibit the central vortex formation). Several reports dealing with flow structures generated by radial impellers are available in the literature. Campolo et al. (2003) described the trajectories of tracers at $Re = 48{,}000$ produced by a Rushton turbine, and Rivera et al. (2004) reported the formation of two symmetrically segregated zones at $Re = 18$. Cooke and Heggs (2005) found that the Scaba impeller produces higher axial flow than the Rushton impeller, and Kovács et al. (2001) concluded that the Scaba impeller demands less power in comparison to the Rushton turbine. All these works have many similarities. They describe the stirring mechanisms but they are limited to the study of a single phase.

Laurenzi et al. (2009) compared the flow structures produced in a stirred tank for a single phase with diluted liquid–liquid dispersion but in their study the mechanism of droplet formation was not discussed. The studies conducted for oil-in-water dispersions (Calabrese et al., 1986a; Zhou and Kresta, 1998: Lovick et al., 2005) did not focus on the state before drops saturate the system. It is worth mentioning that a review of liquid–liquid mixing in stirred vessels has been recently published (Afshar Ghotli et al., 2013). Limited information is available about the formation and evolution of filaments in contact devices. Moreover, the effect of flow properties on the formation of drops under turbulent conditions needs to be further studied. Loth (2008) summarized the deformation conditions of isolated drops in creeping flows in terms of the Weber number and Reynolds number; however, the laminar flow conditions discussed here are far from those generated in a stirred tank. The breakage mechanism of a viscous droplet was studied by Andersson and Andersson (2006) by comparing the deformation process experienced by a drop and the one of an air bubble injected in a fully turbulent flow along a straight pipe.

To the best of our knowledge, few studies dealing with filaments deformed and transported by turbulent flows have been reported, while no reports dealing with filaments submerged in liquid–liquid dispersions in stirred tanks have been published. In the present study, analogous mechanisms are described and reproduced inside a stirred tank. The structure and properties of the flow generated by a Scaba impeller under turbulent conditions and single phase inside a stirred tank have been determined and related to the structures formed during the fragmentation of viscous filaments. Finally, a mechanism describing the drop size reduction process is proposed.

Methods and Materials

Experimental Setup

The experimental setup is shown in Figure 1. Experiments were conducted in a flat bottom cylindrical tank made of glass with an inner diameter $T = 0.135$ m. The liquid volume was $V_L = 1$ L and four baffles of width $T/10$ were equally spaced and fixed inside the tank. A Scaba impeller of diameter $d = \frac{1}{2}T$, consisting of a thin disc and six half-tube blades, was used (Figure 1(a)). The impeller was place at a distance $c = \frac{1}{2}H$ from the vessel bottom, where H is the liquid level. To avoid optical distortion produced by the

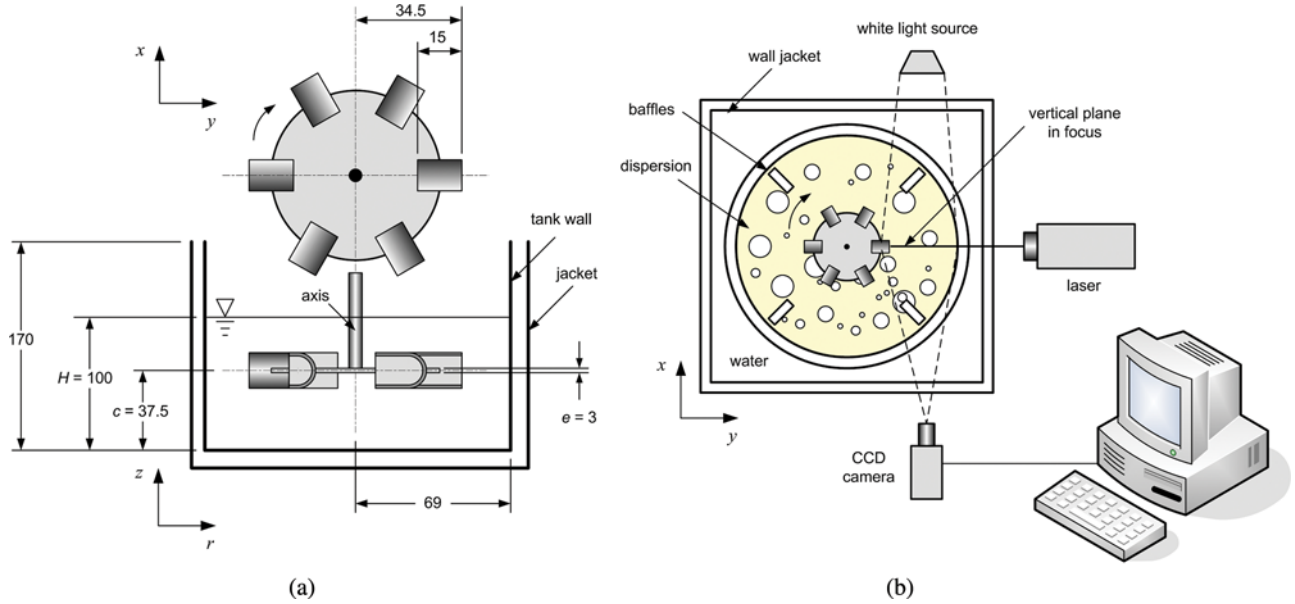

Fig. 1. Experimental setup: (a) Scaba impeller (dimensions in mm); (b) array for high-speed video recording and PIV.

curvature of the cylindrical vessel, a square jacket containing water was used. All experiments were conducted at room temperature (22°C) and no surfactants were employed.

For the continuous phase, distilled water was used ($\rho = 1000\,\mathrm{kg \cdot m^{-3}}$, $\mu = 1.0\,\mathrm{mPa \cdot s}$). A small volume ($\varphi = 1\%\ v/v$) of castor oil ($\rho = 960\,\mathrm{kg \cdot m^{-3}}$, $\mu = 560\,\mathrm{mPa \cdot s}$, surface tension $\sigma_s = 39\ \mathrm{mN \cdot m^{-1}}$) was used as the dispersed viscous phase and located on the water surface. The viscosity ratio of oil to water was 560. The interfacial tension between oil and water was $\sigma_i = 21\,\mathrm{mN \cdot m^{-1}}$ at 20°C (Fisher et al., 1985).

The Reynolds number in stirred tanks is defined as

$$\mathrm{Re} = \frac{\rho N d^2}{\mu} \tag{1}$$

where d is the impeller diameter, N is the rotational speed, and ρ and μ are the density and the dynamic viscosity, respectively. For the present study $Re = 24{,}000$.

The specific power consumption was determined using an air bearing dynamometer by measuring the torque generated by the impeller agitating the working fluid contained in the tank, which rests in a frictionless surface (Ascanio et al., 2004). For the Reynolds number and the work volume (1 L) considered in this study, the specific power was $P/V = 0.46\,\mathrm{W \cdot m^{-3}}$.

Video Recordings and Velocity Measurements

The evolution of the dispersion process was followed by image sequence using a high-speed Charge-Coupled Device (CCD) camera (Redlake Motion Pro HS-4) with an Auto Focusing micro Nikkor 60 mm 1:2.8D lens (Nikon, Japan). Video was recorded for a half plane rz assuming vertical symmetry. The setup was backlighted using a 300 W incandescent filament and a diffuser. All videos were taken at 400 frames/s and a 512×512 pixel image size corresponding to a surface of 60 $\mathrm{cm^2}$. A diagram showing the region studied with the high-speed camera is given in Figure 1(b).

The velocity vector fields in the rz plane were obtained with a particle image velocimetry (PIV) system, which consisted of a high-speed camera Megaplus, Model ES 1.0 (Roper Scientific MASD Inc.) and an Auto Focusing Micro Nikkor 60 mm 1:2.8 D lens (Nikon, Japan). The laser light was generated with a *Solo III PIV* laser (New-Wave, Freemont, CA) at 15 Hz and a wavelength of 532 nm (green light). The *Flow Manager* software, from Dantec Dynamics, was used to control the system and to process the image sequences. Silver-coated glass spheres of 10 μm were used as light reflective tracers. The velocity vector fields were obtained with a standard cross-correlated technique considering 32×32 interrogation windows, with a 50% overlap. A total of 1000 pairs of images were processed to obtain the velocity average ($\bar{v}$) and moving average and filter validations were applied to the resulting fields. The time step between photos was 300 ms. All data were processed with Matlab®.

Turbulence Intensity and Vorticity Field

The instantaneous velocity (v) is defined by

$$v = \bar{v} + v' \tag{2}$$

where $\bar{v}$ refers to the time-average velocity and v' is the fluctuating part that can be computed as the standard deviation of the velocity:

$$v' = \left\{ \sum \frac{(v_i - \bar{v})^2}{n} \right\}^{1/2} \tag{3}$$

The turbulence intensity has been used for studying chaotic flows under the turbulent regime (Mathieu and Scott, 2000). Turbulent flows are characterized for high levels of fluctuating vorticity, which measures the rotation status of a fluid element (Wu et al., 2006). Vorticity was computed as the curl of the mean velocity vector:

$$\omega = \nabla x\, \bar{v} \tag{4}$$

Stretching Efficiency

The stretching efficiency (Devals et al., 2008; Sanjuan-Galindo et al., 2011) denoted as α can be computed as:

$$\alpha = \frac{\dot{\gamma}}{\dot{\gamma} + \dot{\omega}} \tag{5}$$

where $\dot{\gamma}$ represents the modulus of the rate-of-strain tensor ($\underline{\dot{\gamma}}$) and $\dot{\omega}$ represents the norm of the vorticity tensor ($\underline{\dot{\omega}}$). Tensors $\underline{\dot{\gamma}}$ and $\underline{\dot{\omega}}$ are defined by Equations (6) and (7), respectively

$$\underline{\dot{\gamma}} = \frac{1}{2}\left[\nabla \bar{v} + (\nabla \bar{v})^T\right] \tag{6}$$

$$\underline{\dot{\omega}} = \frac{1}{2}\left[\nabla \bar{v} - (\nabla \bar{v})^T\right] \tag{7}$$

where $\nabla \bar{v}$ is defined as follows:

$$\nabla \bar{v} = \frac{\partial \bar{v}}{\partial x_k} e_k \ for\ k = r, z \tag{8}$$

Streamlines

Streamlines are determined by

$$\frac{dx_i}{v_i} = \frac{dx_j}{v_j} \ for\ i \text{ or } j = r, z \tag{9}$$

Results

Flow Patterns

In order to understand the performance of the complex dynamics of the immiscible viscous-phase, the velocity

field produced by the Scaba impeller is first described. Even though the flow field presented corresponds to a single phase, it is still valid for low concentration of castor oil (i.e., 1% v/v). Laurenzi et al. (2009) demonstrated that the flow structures obtained for low-concentration single-phase dispersions are quite similar to those obtained with single-phase liquids. Moreover, the velocity fields and the flow properties will help to explain the viscous-phase deformation process from oil-phase immersion to drops generation.

Figure 2(a) shows the velocity vector field and the scalar magnitude obtained in the vertical rz plane at $Re = 24{,}000$. The velocity pattern agrees with the results presented by Kovács et al. (2001), Khopkar et al. (2004), and Cooke and Heggs (2005), who also described the advantages observed when using Scaba impellers. However, in the present study attention has been paid to the core of the curved blades where the velocity vectors are highly convergent. Khopkar et al. (2004) and Kovács et al. (2001) suggested that the flow discharged by a half-pipe blade is concentrated in the impeller radial direction. It should be noted that this flow structure does not always appear with radial impellers having flat blades like a Rushton turbine, which produces mainly parallel velocity vectors (see for instance Baldi and Yianneskis (2004) and Laurenzi et al. (2009)).

Figure 2(b) exhibits the streamlines in the vertical rz plane (shown as black lines) compared with the velocity field (shown as color lines) at $Re = 24{,}000$. The flow structure observed in this figure is characterized by two toroidal structures below and above the impeller, which are typical of radial impellers. Zalc et al. (2002), Khopkar et al. (2004), and Noui-Mehidi et al. (2008) identified similar structures working in a wide range of flow regimes (20 <

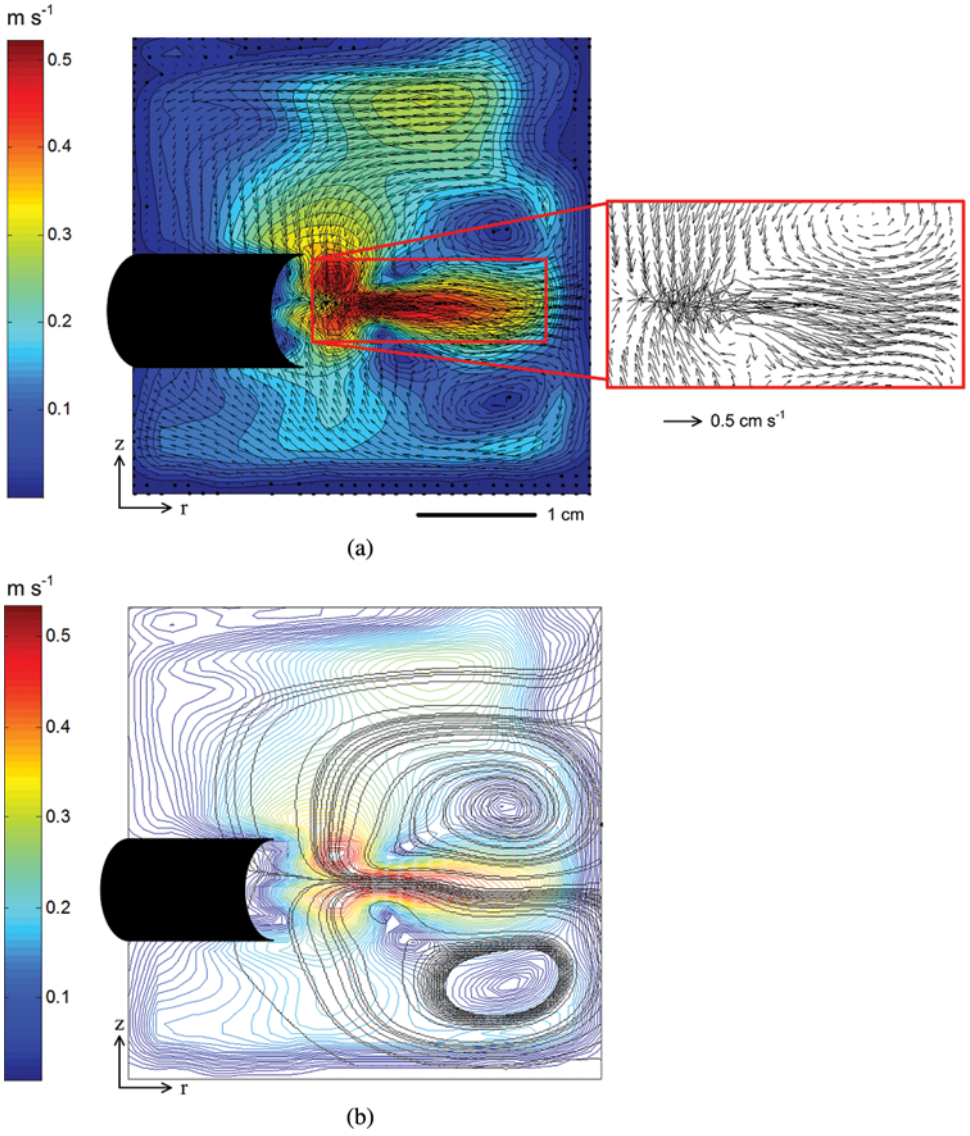

Fig. 2. Time average measurements at $Re = 24{,}000$: (a) velocity vector field and the velocity magnitude; (b) streamlines (black lines) and the velocity magnitude (color lines).

$Re < 45{,}000$). In the present case, the maximum liquid velocity ($|\bar{v}|_{max} \approx 0.5\,\mathrm{ms}^{-1}$) is found in the region of the blade discharge. This magnitude represents a half of the impeller tip velocity, which has been estimated as $v_{tip} = d \cdot \pi \cdot N = 1\,\mathrm{m/s}$. On the other hand, the minimum velocities ($v < 0.05\,\mathrm{m/s}$) have been observed in the core of both the toroidal structures, which are known as isolated mixing regions and are susceptible to retain a volume of the viscous phase in a stagnation region. The flow in the rest of the liquid bulk is mainly characterized by a mean velocity $|\bar{v}|$ of the order of $0.1\,\mathrm{m} \cdot \mathrm{s}^{-1}$. This value is small enough to slightly deform the viscous phase, which suggests a rotational flow with poor mass and energy transfer.

Oil-Phase Dragging and Formation of Viscous Filaments

In the beginning of the dispersion process, the viscous phase rests on the liquid surface. When the impeller started rotating, the oil phase (a less-dense and low-concentrated liquid, $\frac{\rho_{oil}}{\rho_{H_2O}} < 1, \varphi = 1\%\ v/v$) is sucked toward the impeller by the low pressure induced by the rotation. A visual description of the dragging process is shown in Figure 3. The images show how the oil phase is dragged into the liquid bulk producing thick oil threads that become twisted and helically driven around the shaft. Several kinds of amorphous structures are expelled in the radial direction including thin and stretched filaments. The viscous-phase dragging process is compared with the flow pattern at time t_4 in Figure 3(d).

Even though oil filaments are notoriously more viscous than water ($\mu_{\mathrm{oil}}/\mu_{\mathrm{H_2O}} = 560$), such structures are easily perturbed by the continuous-phase flow. As a result of these perturbations, filaments become thinned, folded, and fragmented. Four types of perturbations have been identified: (a) intermittences in the radial velocity, (b) turbulent fluctuation, (c) rotation, and (d) stretching. Each of these phenomena is described in the following lines.

Intermittences in the Radial Velocity

The flow ejected by the impeller blades is unsteady in the radial direction. Depending on the relative position of the blade, intermittent jets are produced. A schematic representation of such a jet is shown in Figure 4. Considering a reference point, jets appear with a frequency which is a function of the number of blades (n) and the rotational speed (N): $f = \frac{1}{n}N = 0.8\,\mathrm{s}^{-1}$. The filaments dragged by the impeller blades and expelled in the radial direction onto the tank wall are perturbed as a result of these periodic impulses. However, the pushing energy provided by the blade is quickly dissipated.

The linear velocity at which the filament is ejected onto the liquid was measured for 60 ms and results are shown in Figure 5(a) for two different filaments. The filament velocity was normalized with the impeller tip speed; peak values are related to the maximum energy delivered by the jet, while valleys are related to the minimum energy when the impeller blades do not produce a jet. Once the filament escapes from the blade (i.e., $r/R = 0.8$, close to the tank wall), the jet strength decreases, and the filament is no longer radially displaced and it is perturbed by other causes as interface instabilities. Figure 5(b) illustrates an example of this periodic perturbation.

Turbulence Fluctuations

Turbulent flows enhance transport processes and exhibit strong diffusivity (Mathieu and Scott, 2000). Calabrese et al. (1986a) stated that shear forces and turbulence fluctuations govern the flow in the impeller neighborhood. In the present work, the visual evidence shows the effects of the turbulence onto the dispersed phase. Figure 6(a) shows the scalar field of the turbulent intensity (v') in the vertical plane rz at $Re = 24{,}000$. It is important to point out that high values of turbulent intensity, that is $v' = 0.5\,\mathrm{m} \cdot \mathrm{s}^{-1}$, are observed near the blade tip, which agree with the converging flow (previously shown in Figure 2(a)). Close to the tank wall, in the impeller discharge direction, the turbulent intensity decreases, that is, $0.1\,\mathrm{m} \cdot \mathrm{s}^{-1} < v' < 0.3\,\mathrm{m} \cdot \mathrm{s}^{-1}$, while the flow in the rest of the liquid bulk exhibits the lowest turbulence intensity, that is $v' \approx 0.1\,\mathrm{m} \cdot \mathrm{s}^{-1}$, suggesting that the flow is mostly rotational, as discussed below.

Figure 6(b) shows a U-shaped filament. These structures are produced randomly in the zone of high turbulence intensity, that is, v' of the order of $0.5\,\mathrm{m} \cdot \mathrm{s}^{-1}$. Some filaments are also stretched, deformed, and fragmented, which are the steps preceding the formation of oil drops. Some other filaments are simply dragged and sent away from the impeller zone. The hairpin filaments resemble the numerical description presented by Yarin (1997). However, the author investigated the folding

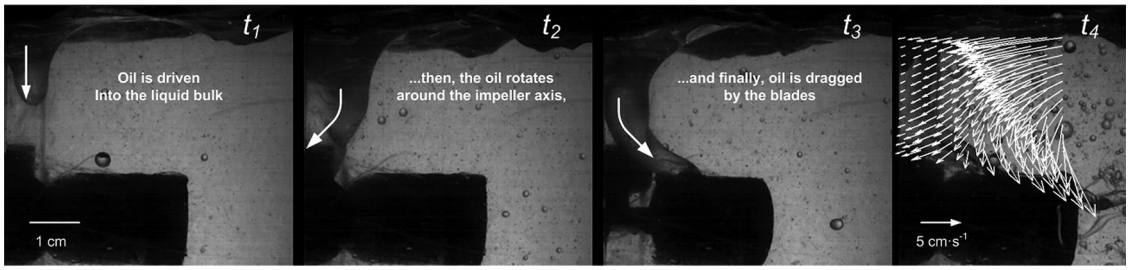

(a) (b) (c) (d)

Fig. 3. Time-average velocity pattern governing the process (oil dragging from the surface into liquid bulk): (a) $t_1 = 0\,\mathrm{ms}$; (b) $t_2 = 195\,\mathrm{ms}$; (c) $t_3 = 210\,\mathrm{ms}$; (d) $t_4 = 385\,\mathrm{ms}$ with the velocity field.

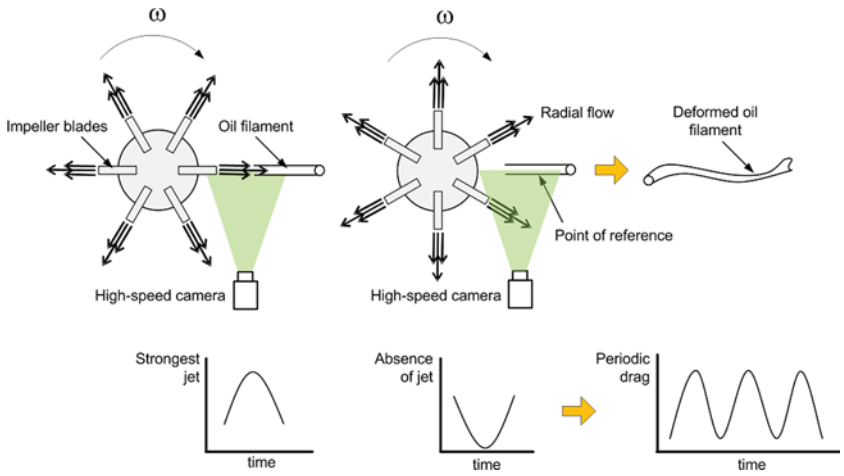

Fig. 4. Schematic representation of the intermittent flow produced by the rotation of the impeller.

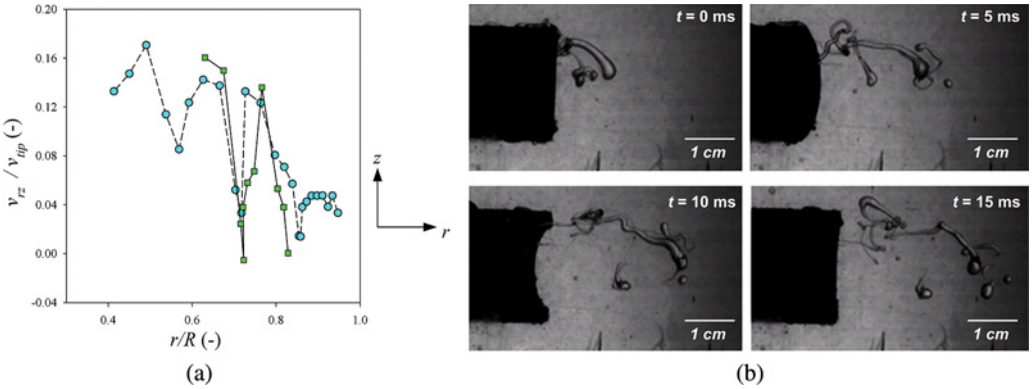

Fig. 5. (a) Normalized velocity of two filament points displaced in the *rz* plane measured for 60 ms (v_{tip} refers to the impeller tip velocity, and *R* represents the tank radius); (b) filaments disturbed by the radial velocity intermittence from 0 to 15 ms.

of a filament under laminar regime, which differs from the turbulent conditions used in the present work.

Buckling and accumulation are observed when the filaments are thrown against the shear-free surface (Skorobogatiy and Mahadevan, 2000; Lueptow and Lueptow, 2012). Our results show that filaments discharged into a turbulent flow may exhibit elongation, thinning, or rupture. In the case of filaments expelled to a non-turbulent

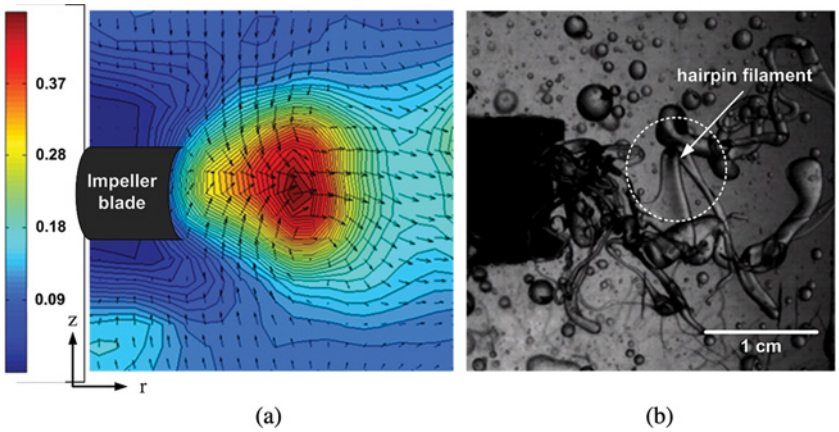

Fig. 6. (a) Time average measurements of the turbulence intensity and the velocity vector field at $Re = 24{,}000$. (b) Random production of hairpin filaments in the zone of high turbulence intensity.

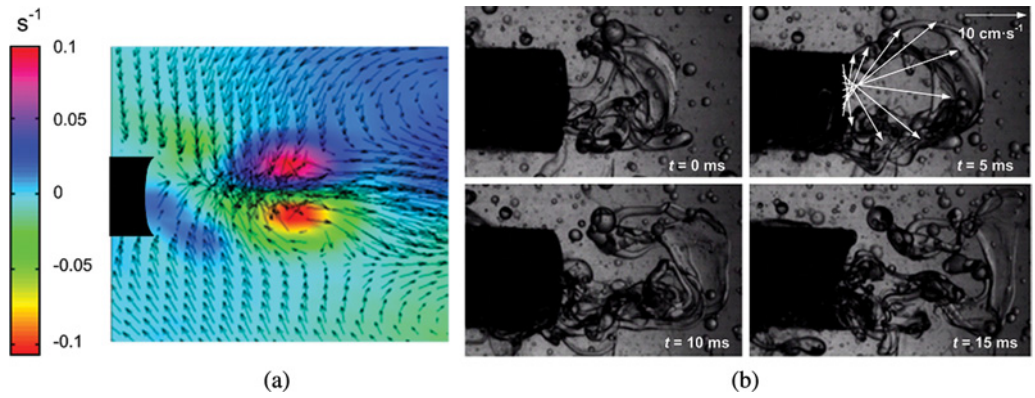

Fig. 7. Influence of vortex structure on the formation of threads expelled by impeller blades: (a) vorticity 1/s and velocity field; (b) filaments formed by the blades and velocity field in the filament formation ($t = 5$ ms).

flow, they simply recoil, adopt spheroidal shapes, or remain stable. Inside a stirred tank, the last two cases are possible due to the flow pattern heterogeneity, which may exhibit turbulent and non-turbulent conditions.

Rotation

In Figure 7(a), two swirling regions of opposite vorticity signs with absolute magnitudes of 0.06 are identified. These regions are located symmetrically in both sides of the impeller disc near the impeller blade discharge. Although, turbulent flows exhibit vorticity, the effects of the vortex field on a viscous phase have not been deeply studied yet. In the vortex zone, the inertial forces dominate over the viscous forces because the flow is inertial. The oil phase expelled by the blades is attracted by the low pressure of the vortex cores and driven by the radial flow discharged by the impeller. These forces lead to the formation of complex structures (Figure 8(b)). Velocity vectors have been superimposed on the image to explain its influence. These viscous thin sheets are unstable in presence of the turbulent flow and highly sensitive to rupture. It should be noted that such structures are shaped by a tridimensional and turbulent flow. These structures are no longer produced at less turbulent regions.

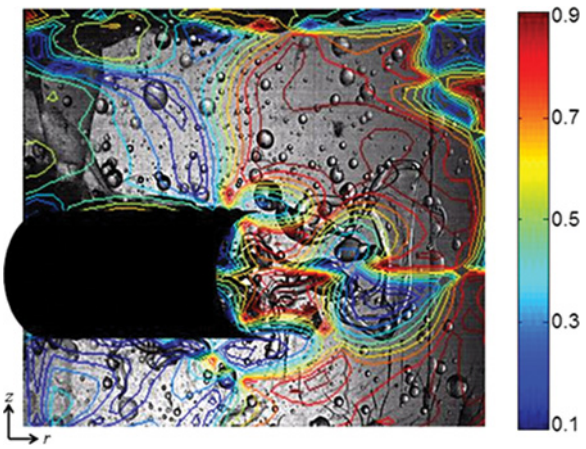

Fig. 8. Viscous structures deformation and the stretching efficient contour map (dimensionless) at $Re = 24{,}000$.

This stage ends with the formation of numerous drops with a wide size distribution.

Stretching

A stretched fluid volume experiences dimension changes as a function of time (Ottino, 1989; Voth et al., 2002). Stretching produced in stirred tanks has been modeled estimating the stretching efficiency of laminar flows (Heniche et al., 2005; Devals et al., 2008). Let us recall the interpretation of the values of the stretching efficiency (α, Equation (7)). For $\alpha = 0$ ($\dot{\gamma} = 0$, $\dot{\omega} \neq 0$), the flow is purely rotational. Flow is considered as a pure simple shear flow for $\alpha = 0.5$ ($\dot{\gamma} = \dot{\omega}$). Finally, for $\alpha = 1.0$ ($\dot{\gamma} \neq 0$, $\dot{\omega} = 0$), the flow is considered to be purely extensional. The local stretching efficiency obtained in the present work is presented in Figure 8. This image has been superimposed on the viscous fluid volume ejected from the blade. The range of the stretching efficiency is $0.1 < \alpha < 0.9$. In the field of α, at least two zones can be identified to explain where the oil phase is fragmented in the liquid bulk. In the first region (i.e., the left side of the figure) α has smaller values (i.e., $\alpha < 0.4$, marked by blue lines), which characterizes a mainly rotational flow. In this zone, little viscous-phase fragmentation is observed. In the second region (i.e., the right side of the figure), the stretching efficiency reaches larger values (i.e., $\alpha > 0.6$,

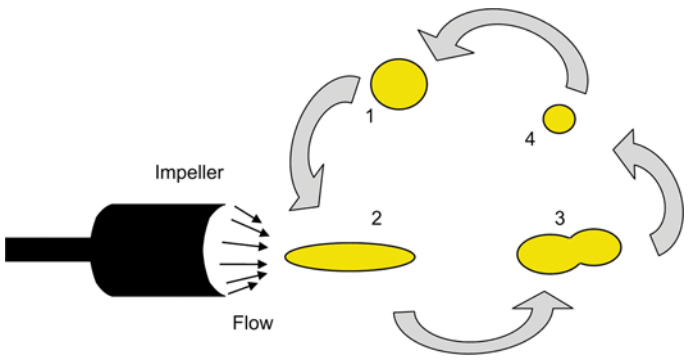

Fig. 9. Proposed mechanism to generate viscous droplets: (1) mother drop; (2) deformed drop (filament); (3) drop partition; (4) daughter drop.

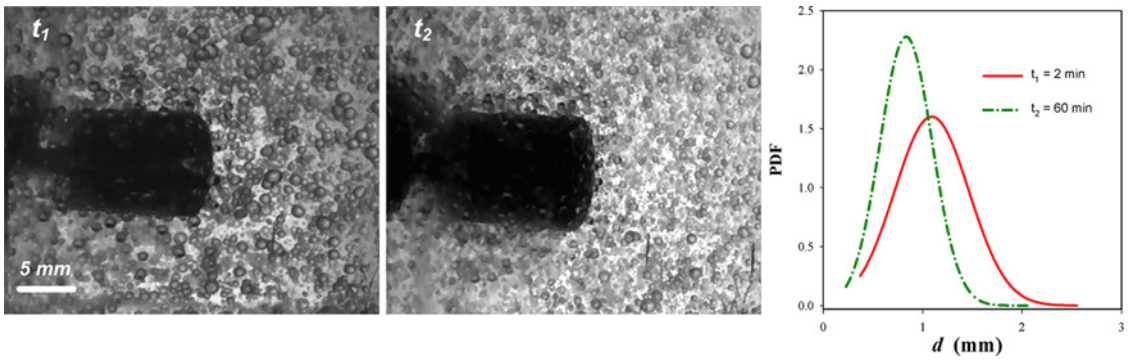

Fig. 10. High-speed images of an oil-in-water dispersion produced in a stirred tank from rest state: (a) $t_1 = 2$ min; (b) $t_2 = 60$ min; (c) probability density function of drop diameter obtained at t_1 and t_2.

marked by yellow and red lines mainly). This zone has larger values of shear and extension. Such flow behavior and properties have different effects in the viscous phase. For instance, in the zone where $\alpha > 0.6$, the viscous phase becomes elongated, fragmented, or experiences size reduction. Conversely, in the low stretching zone, where $\alpha < 0.4$, those fragmented structures recoil and spheroidal fluid elements remain unchanged and rotate around the shaft. Such flow behavior corresponds to those phenomena registered using high-speed video. For instance, Figure 8 shows the time when a filament becomes elongated as it is expelled by the blade to a high stretching zone ($\alpha \approx 0.7$). The low stretching zone is characterized also for its low turbulence. These results are helpful to understand the performance of the half-pipe blade.

Droplet Size Distribution

The drop size distribution produced in stirred tanks has been the center of attention in numerous publications (Calabrese et al., 1986a; Chatzi et al., 1991, Zhou and Kresta, 1998; Sajjadi et al., 2002; Lovick et al., 2005). However, the mechanism of breakage in a stirred tank has not been completely clarified. Zhou and Kresta (1998) proposed that drops are broken when they gain enough energy to compensate for the increase of the total surface area. In a different work, Andersson and Andersson (2006) documented how a single viscous drop is deformed and broken as it is injected into a developed turbulent flow along a straight pipe. Similar features have been recognized in stirred tanks. Drop breakage follows a four-step mechanism (illustrated in Figure 9), in which the first step is when mother drops enter the zone characterized as turbulent with high stretching coefficients; in a second step, the drops experience stretching and some necks are produced; such deformed drops are capillary unstable and they are easily fragmented (third step); finally, daughter drops are dispersed in a zone with low turbulence and weak stretching conditions. The cycle is repeated until reaching the steady state as claimed by Chatzi et al. (1991) and Liu and Li (1999). This mechanism is in agreement with the observations of Cristini et al. (2003), who considered that drops are broken by the shear forces generated in the blade discharge. Those segregated drops (i.e., drops moving faraway from the blade discharge) are not disrupted and remain stable. Finally, the mechanical impacts (with the impeller, baffles or the tank wall) could also have a secondary role in drop breakage.

In the beginning of the process, breakage occurs more often because big drops are more unstable than the smaller ones. It is nearly impossible for all drops achieve a uniform size distribution and there is a debate about drops size. The minimum size has been predicted considering the Kolmogorov theory (Liu and Li, 1999), but others have discarded this prediction (Zhou and Kresta, 1998; Cristini et al., 2003). Mathematical relations have been suggested to predict the biggest drop or the mean size, particularly for several silicon types or petroleum by-products (Calabrese et al., 1986b; Wang and Calabrese, 1986; Zhou and Kresta, 1998); however, oils used in biochemical processes, such as castor oil, have been less studied.

The drop size and distribution at two different times have been compared with the *in situ* measurements of about 500 drops for two different states. Figure 10(a) shows the first state captured once the filaments were disrupted (i.e., $t = 2$ min), while the second state has been taken after stirring for 1 h at constant temperature (Figure 10(b)). For both cases, the probability density function is shown in Figure 10(c). The initial state is characterized by big size drops and wider dispersion. The largest diameter, d_{max}, is of the order of 2.5 mm, while the smallest drop, d_{min}, about 0.23 mm. Each peak represents the average diameter for each state, that is $d_{av} = 1.1$ mm for the initial state, and $d_{av} = 0.834$ mm is for the steady state ($t = 60$ min). Drop collision and coalescence are other phenomena involved in the drop size definition; however, they occur mainly in high-concentrated dispersions (Coulaloglou and Tavlarides, 1976).

Conclusions

In the present study, the process to disperse a viscous fluid in a stirred tank was discussed, and the main features of the flow were identified with the process of the drop formation. Before oil drops are formed, the viscous phase adopts filaments-like structures easily perturbed by the flow

properties. The radial impeller generates two eddies, distributed above and below the impeller centerline, which contain two local zones of low velocity able to segregate a viscous-phase volume. In the opposite case, the maximum liquid velocity is produced in the blade discharge, where flow is highly turbulent. The influence of four flow properties causing filament instabilities, such as intermittences in the radial velocity, turbulence, rotation, and stretching, was discussed. In the first case, filaments receive intermittent pulses producing elongation and buckling. The turbulent flow ejected from the blades exhibits the formation of vortex rings, which produces highly unstable structures that are randomly deformed. The stretching coefficient distribution was presented to learn the possible zones where deformation takes place. This information can be useful to improve the design and operation of two-phase contact devices. A periodic mechanism to produce drops size fragmentation was discussed. It starts when drops in the blade flow are deformed until necking, thereafter they are broken and two daughter droplets are generated. The effect of this process in the drop size was evaluated. To our knowledge, this is the first work that documents the viscous filament generation in turbulent flow conditions in a stirred tank comparing such events with the velocity patterns. This experiment opens the possibility to further investigate this phenomenon to test some other fluids or some other techniques.

Funding

R. Sanjuan-Galindo thanks the PhD scholarship provided by the National Council for Science and Technology of Mexico. The financial support of DGAPA-UNAM through the grant PAPIIT 108312 is highly acknowledged. We also acknowledge the technical assistance provided during this investigation by Dr. A. Hidalgo-Millán (UAN) and M.A. Bazan (UNAM).

References

Afshar Ghotli, R., Raman, A. A. A., Ibrahim, S., and Baroutian, S. (2013). Liquid-liquid mixing in stirred vessels: a review, *Chem. Eng. Commun.*, **200**, 595–627.

Andersson, R., and Andersson, B. (2006). On the breakup of fluid particles in turbulent flows, *AIChE J.*, **52**, 2020–2030.

Ascanio, G., Castro, B., and Galindo, E. (2004). Measurement of power consumption in stirred vessels—A review, *Chem. Eng. Res. Des.*, **82**(A9), 1282–1290.

Baldi, S., and Yianneskis, M. (2004). On the quantification of energy dissipation in the impeller stream of a stirred vessel from fluctuating velocity gradient measurements, *Chem. Eng. Sci.*, **59**, 2659–2671.

Calabrese, R. V., Wang, C. Y., and Bryner, N. P. (1986a). Drop breakup in turbulent stirred-tank contactors, Part I: Effect of dispersed-phase viscosity, *AIChE J.*, **32**, 657–666.

Calabrese, R. V., Wang, C. Y., and Bryner, N. P. (1986b). Drop breakup in turbulent stirred-tank contactors. Part III: Correlations for mean size and drop size distribution, *AIChE J.*, **32**, 677–681.

Campolo, M., Sbrizzai, F., and Soldati, A. (2003). Time-dependent flow structures and Lagrangian mixing in Rushton-impeller baffled-tank reactor, *Chem. Eng. Sci.*, **58**, 1615–1629.

Chatzi, E. G., Boutris, C. J., and Kiparissides, C. (1991). On-line monitoring of drop size distribution in agitated vessels. 1. Effect of temperature and impeller speed, *Ind. Eng. Chem. Res.*, **30**, 536–543.

Cooke, M., and Heggs, P. J. (2005). Advantages of the hollow (concave) turbine for multi-phase agitation under intense operating conditions, *Chem. Eng. Sci.*, **60**, 5529–5543.

Coulaloglou, C. A., and Tavlarides, L. L. (1976). Drop size distribution and calescence frequencies of liquid-liquid dispersions in flow vessels, *AIChE J.*, **22**, 289–297.

Cristini, V., Blawzdziewicz, J., Loewenberg, M., and Collins, L. R. (2003). Breakup in stochastic Stokes flows: Sub-Kolmogorov drops in isotropic turbulence, *J. Fluid Mech.*, **492**, 231–250.

Devals, C., Heniche, M., Takenaka, K., and Tanguy, P. A. (2008). CFD analysis of several design parameters affecting the performance of the Maxblend impeller, *Comput. Chem. Eng.*, **32**, 1831–1841.

Duclaux, V., Clanet, C., and Quéré, D. (2006). The effects of gravity on the capillary instability in tubes, *J. Fluid Mech.*, **556**, 217–226.

Eggers, J., and Villermaux, E. (2008). Physics of liquid jets, *Rep. Prog. Phys.*, **71**, 036601.

Fisher, L. R., Mitchell, E. E., and Parker, N. S. (1985). Interfacial tensions of commercial vegetable oils with water, *J. Food Sci.*, **50**, 1201–1202.

Hagedorn, J. G., Martys, N. S., and Douglas, J. F. (2004). Breakup of a fluid thread in a confined geometry: Droplet-plug transition, perturbation sensitivity, and kinetic stabilization with confinement, *Phys. Rev. E*, **69**, 056312.

Heniche, M., Tanguy, P. A., Reeder, M. F., and Fasano, J. B. (2005). Numerical investigation of blade shape in static mixing, *AIChE J.*, **51**, 44–58.

Khopkar, A., Aubin, J., Rubio-Atoche, C., Xuereb, C., Le Sauze, N., Bertrand, J., and Ranade, V. V. (2004). Flow generated by radial flow impellers: PIV measurements and CFD simulations, *Int. J. Chem. Reactor Eng.*, **2**, A18.

Kovács, T., Trägårdh, C., and Fuchs, L. (2001). Flow and turbulence in the discharge of radial pumping turbines: Influence of the turbine type, *Chem. Eng. Technol.*, **24**, 1035–1044.

Laurenzi, F., Coroneo, M., Montante, G., Paglianti, A., and Magelli, F. (2009). Experimental and computational analysis of immiscible liquid–liquid dispersions in stirred vessels, *Chem. Eng. Res. Des.*, **87**, 507–514.

Le Merrer, M., Seiwert, J., Quéré, D., and Clanet, C. (2008). Shapes of hanging viscous filaments, *Europhys. Lett.*, **84**, 56004.

Loth, E. (2008). Quasy-steady shape and drag of deformable bubbles and drops, *Int. J. Multiphase Flow*, **34**, 513–546.

Lovick, J., Mouza, A. A., Paras, S. V. Lye, G. J., and Angeli, P. (2005). Drop size distribution in highly concentrated liquid-liquid dispersions using a light back scattering method, *J. Chem. Technol. Biotechnol.*, **80**, 545–552.

Liu, S., and Li, D. (1999). Drop coalescence in turbulent dispersions, *Chem. Eng. Sci.*, **54**, 5667–5675.

Lueptow, K. L., and Lueptow, R. M. (2012). Stretched coiling instability. *Am. Phys. Soc.*, Division of Fluid Dynamics 2012 Image Gallery. http://www.aps.org/units/dfd/pressroom/gallery/2012/lueptow12.cfm (visited on April 2013).

Mathieu, J., and Scott, J. (2000). *An Introduction to Turbulent Flow*, Cambridge University Press, Cambridge, UK.

Noui-Mehidi, M. N., Ohmura, N., Wu, J., Nguyen, B. V., Nishioka, N., and Takigawa, T. (2008). Characterization of isolated mixing regions in a stirred vessel, *Int. J. Chem. Reactor Eng.*, **6**, A25.

Oliveira, M. S. N., and McKinley, G. H. (2005). Iterated stretching and multiple beads-on-a-string phenomena in dilute solutions of high extensible flexible polymers, *Phys. Fluids.*, **17**, 071704.

Ottino, J. M. (1989). *The Kinematics of Mixing: Stretching, Chaos and Transport*, Cambridge University Press, New York, NY.

Plateau, J. (1849). Statique expérimentale et théorique des liquides soumis aux seules forces moléculaires (Gaitier-Villars, Paris, 1873), *Acad. Sci. Bruxelles Mém*, **23**, 5.

Rayleigh, L. (1892). On the instability of cylindrical fluid surfaces, *Phil. Mag.*, **34**, 177–180.

Ribe, N. M. (2004). Coiling of viscous jets, *Proc. R. Soc. London A*, **460**, 3223–3239.

Rivera, C., Heniche, M., Ascanio, G., and Tanguy, P. A. (2004). A virtual finite element model for centered and eccentric mixer configurations, *Comput. Chem. Eng.*, **28**, 2459–2468.

Sajjadi, S., Zerfa, M., and Brooks, B. W. (2002). Dynamic behavior of drops in oil/water/oil dispersions, *Chem. Eng. Sci.*, **57**, 663–675.

Sanjuan-Galindo, R., Heniche, M., Ascanio, G., and Tanguy, P. A. (2011). CFD investigation of new helical ribbon mixers bottom shapes to improve pumping, *Asia-Pac. J. Chem. Eng.*, **6**, 181–193.

Skorobogatiy, M., and Mahadevan, L. (2000). Folding of viscous sheets and filaments, *Europhys. Lett.*, **52**, 532–538.

Tjahjdadi, M., and Ottino, J. M. (1991). Stretching and breakup of droplets in chaotic flows, *J. Fluid Mech.*, **232**, 191–219.

Voth, G. A., Haller, G., and Gollub, J. P. (2002). Experimental measurements of stretching fields in fluid mixing, *Phys. Rev. Lett.*, **88**, 254501.

Wang, C. Y., and Calabrese, R. V. (1986). Drop breakup in turbulent stirred-tank contactors. Part II: relative influence of viscosity and interfacial tension, *AIChE J.*, **32**, 667–676.

Wu, J. Z, Ma, H. Y., and Zhou, M. D. (2006). *Vorticity and Vortex Dynamics*, Springer-Verlag, Heidelberg.

Yarin, A. L. (1997). On the mechanism of turbulent drag reduction in dilute polymer solutions: Dynamics of vortex filaments, *J. Non-Newtonian Fluid Mech.*, **69**, 137–153.

Zalc, J. M., Szalai, E. S., Alvarez, M. M., and Muzzio, F. J. (2002). Using CFD to understand chaotic mixing in laminar stirred tanks, *AIChE J.*, **48**, 2124–2134.

Zhou, G., and Kresta, S. M. (1998). Correlation of mean drop size and minimum drop size with the turbulence energy dissipation and the flow in an agitated tank, *Chem. Eng. Sci.*, **53**, 2063–2079.